Lifetime measurements of medium-heavy Λ hypernuclei

H. Park,* H. Bhang, and M. Youn†
Department of Physics, Seoul National University, Seoul 151-742, Korea

O. Hashimoto, K. Maeda, Y. Sato, and T. Takahashi
Department of Physics, Tohoku University, Aoba-ku, Sendai, Miyagi 980-77, Japan

K. Aoki, Y. D. Kim,‡ H. Noumi, K. Omata, H. Outa, M. Sekimoto, and T. Shibata
High Energy Accelerator Research Organization (KEK), Tsukuba, Ibaraki 305-0801, Japan

T. Hasegawa,§ H. Hotchi, and Y. Ohta
Graduate School of Science, University of Tokyo, Tokyo 113-0033, Japan

S. Ajimura and T. Kishimoto
Department of Physics, Osaka University, Toyonaka, Osaka 560-0043, Japan
(Received 10 December 1999; published 21 April 2000)

We have measured the lifetimes of the weak decay of ${}^{12}_{\Lambda}$C, ${}^{28}_{\Lambda}$Si, and ${}^{56}_{\Lambda}$Fe hypernuclei which were produced via a (π^+,K^+) reaction at KEK 12-GeV PS. The lifetimes were obtained by direct measurement of the production and decay time of the hypernucleus using a fast timing counter system whose time resolution was about 83 ps. Our results for the lifetimes of ${}^{12}_{\Lambda}$C, ${}^{28}_{\Lambda}$Si, and ${}_{\Lambda}$Fe are 231 ± 15, 206 ± 11, and 215 ± 14 ps, respectively. The lifetimes of ${}^{11}_{\Lambda}$B and ${}^{27}_{\Lambda}$Al with the application of the gate to the p_{Λ} state of the formation spectra of ${}^{12}_{\Lambda}$C and ${}^{28}_{\Lambda}$Si were also determined to be 211 ± 13 and 203 ± 10 ps. From the present work, it was found that the total decay width saturates according to the hypernuclear mass number even at $A\sim12$. This suggests the importance of the proper treatment of the short range nature of the nonmesonic decay of Λ hypernuclei.

PACS number(s): 21.80.+a, 13.30.Eg, 13.75.Ev, 21.10.Tg

I. INTRODUCTION

The weak decay of Λ hypernuclei has been studied over many years since its discovery in 1952 in an emulsion experiment. Hypernuclei are typically produced in excited states (or ground states) through the strangeness production reaction and can reach their ground state through nucleon emission and/or electromagnetic decay. Eventually, they will decay through weak interaction processes which involve the emission of pions or nucleons.

A free Λ hyperon decays mostly into a nucleon and a pion via the weak nonleptonic decay

$$\Lambda\rightarrow\begin{cases} p+\pi^- +37.8\ \text{MeV} & (63.9\%), \\ n+\pi^0+41.1\ \text{MeV} & (35.8\%), \end{cases} \tag{1}$$

with a lifetime of 263 ps. The branching ratios of the two channels are 35.8% and 63.9% [1] and are consistent with a simple calculation from the empirical $\Delta I=1/2$ rule. The energy released in the free Λ decay is about 40 MeV and the corresponding momentum of a nucleon and a pion in their center-of-mass frame is about 100 MeV/c.

When a Λ hyperon is bound in the nucleus, the mesonic decay channel is highly suppressed except for the very light nuclei because of Pauli blocking of the final-state nucleon. Nucleon-induced decay, the so-called nonmesonic decay, becomes dominant. This channel does not occur in the free Λ [2],

$$\Lambda+p\rightarrow n+p+176\ \text{MeV}, \tag{2}$$

$$\Lambda+n\rightarrow n+n+176\ \text{MeV}. \tag{3}$$

The energy release of this decay mode is about 176 MeV and the momentum of each final-state nucleon is about 400 MeV/c, which is much higher than the Fermi momentum. As a result, this decay mode becomes dominant in medium and heavy hypernuclei.

Thus, the total decay width (Γ) and the lifetime (τ) of Λ hypernuclear weak decay can be written

$$\Gamma=\frac{1}{\tau}=\Gamma_{\pi}+\Gamma_{nm}, \tag{4}$$

$$\Gamma_{\pi}=\Gamma_{\pi^-}+\Gamma_{\pi^0}, \tag{5}$$

$$\Gamma_{nm}=\Gamma_{p}+\Gamma_{n}+(\Gamma_{2p2h}), \tag{6}$$

where $\Gamma_{\pi^-(\pi^0)}$ is the partial decay width of $\pi^-(\pi^0)$ mesonic decay, $\Gamma_{p(n)}$ is that of proton-(neutron-) induced nonmesonic

*Present address: High Energy Accelerator Research Organization (KEK), Tsukuba, Ibaraki 305-0801, Japan.
†Present address: University of Houston, Houston, TX 77004.
‡Present address: Department of Physics, Sejong University, Seoul 144-747, Korea.
§Present address: School of Allied Health Sciences, Kitasato University, Sagamihara 228-8555, Japan.

decay, and Γ_{2p2h} is that of the two-nucleon-induced nonmesonic decay which has been suggested [3] but not yet confirmed.

The $\Lambda N \rightarrow NN$ interaction is the strangeness changing $\Delta S=1$ analogy of the weak $NN \rightarrow NN$ interaction responsible for nuclear parity violation [4]. In the case of the $NN \rightarrow NN$ weak interaction, the parity-conserving part is not observable because it is overwhelmed by the strong interaction.

At present, a direct study of the hyperon-nucleon weak interaction is difficult due to the lack of either a hyperon beam or target and the low cross section, even if the time-reversed process $pn \rightarrow \Lambda p$ were to be made possible by new facilities [5]. So nonmesonic decay provides the most practical means to investigate the four-fermion weak vertex and $\Lambda N \rightarrow NN$ weak interaction which occurs only in the nuclear medium.

In addition, one of the most important characteristics of the nonmesonic decay process is the large momentum transfer of about 400 MeV/c. Such a large momentum transfer implies that it probes short distances of the order of 0.5 fm and might, therefore, expose the role of explicit quark degrees of freedom in the nucleus. Furthermore, in investigating the nonmesonic decay of hypernuclei, one can explore the question of whether the $\Delta I=1/2$ rule that governs π mesonic decay applies to nonmesonic decays.

The total decay width (or lifetime) is the observable which can be measured most accurately and interpreted free from the nuclear final-state interaction. The lifetime measurement can be the starting point for obtaining the various observables, e.g., partial decay widths of mesonic or nonmesonic decay, the ratio of proton- to neutron-induced nonmesonic decay rates, etc. In addition, the variation of lifetime with hypernuclear mass number can provide a qualitative understanding of the nuclear medium effects on the baryon-baryon weak interaction.

Table I shows the status of the previous lifetime measurements. For light hypernuclei of $A \leqslant 5$, there are old emulsion data for the lifetimes with large uncertainties. Recently, some counter experiments were performed at BNL [17,16] and KEK [12,13] for ${}^{4}_{\Lambda}$H, ${}^{4}_{\Lambda}$He, and ${}^{5}_{\Lambda}$He hypernuclei. In the medium mass region, there are only two sets of data. Grace *et al.* [17] obtained the lifetimes by applying various gates on excitation energies of the ${}^{12}_{\Lambda}$C hypernucleus. The lifetime of the hypernucleus of $A \sim 16$ was measured at LBL [18] using a ^{16}O beam, but the production of a hypernucleus was not identified explicitly in the experiment. For heavy hypernuclei with $A>200$, there exists some lifetime data using antiproton or proton beams to measure the delayed fission fragments. Recently, the lifetime of the hypernuclear fission fragments from the $p+{}^{238}$U interaction was measured within reasonable uncertainties using a proton beam at COSY [22]. In these measurements for heavy hypernuclei with $A>200$, the hypernuclear production was not explicitly identified. Before the present experiment, there had existed only one measurement in the mass region from $A=12$ to 200, which has large errors and could not identify the hypernuclear formation clearly. The present experiment will provide the lifetimes in this region with clear hypernuclear formation spectra.

TABLE I. The status of the lifetime mesurements.

A	τ (ps)	Ref.	Expt.
${}^{3}_{\Lambda}$H	90^{+220}_{-40}	[6]	Emulsion
	285^{+127}_{-105}	[7]	Emulsion
	128^{+35}_{-26}	[8]	Emulsion
	264^{+84}_{-52}	[9]	Bubble chamber
	246^{+62}_{-41}	[10]	Bubble chamber
${}^{4}_{\Lambda}$H	180^{+250}_{-70}	[6]	Emulsion
	360^{+490}_{-130}	[11]	Emulsion
	268^{+166}_{-107}	[7]	Emulsion
	194^{+24}_{-26}	[12,13]	(K^{-}_{stop},π^{-})
${}^{4}_{\Lambda}$He	228^{+233}_{-129}	[7]	Emulsion
	245 ± 24	[14]	(K^{-},π^{-})
	256 ± 27	[13]	(K^{-}_{stop},π^{-})
${}^{5}_{\Lambda}$He	140^{+190}_{-50}	[6]	Emulsion
	180^{+150}_{-60}	[11]	Emulsion
	251^{+190}_{-73}	[7]	Emulsion
	274^{+60}_{-50}	[15]	Emulsion
	256 ± 21	[16]	(K^{-},π^{-})
${}^{9}_{\Lambda}$Be	201 ± 30	[16]	(K^{-},π^{-})
${}^{11}_{\Lambda}$B	192 ± 22	[17,16]	(K^{-},π^{-})
${}^{12}_{\Lambda}$C	211 ± 31	[17,16]	(K^{-},π^{-})
${}^{16}_{\Lambda}$Z	86^{+33}_{-26}	[18]	^{16}O beam, K^{+} tagging
$\bar{p}+{}^{209}$Bi	250^{+250}_{-100}	[19]	Delayed fission
	$180\pm40\pm60$	[20]	Delayed fission
$e+{}^{209}$Bi	2700 ± 500	[21]	Delayed fission
$\bar{p}+{}^{238}$U	100^{+80}_{-40}	[19]	Delayed fission
	$130\pm30\pm30$	[20]	Delayed fission
$p+{}^{238}$U	240 ± 60	[22]	Delayed fission
$p+{}^{209}$Bi	$145\pm7\pm23$	[23]	Delayed fission

The goals of this experiment were the precise measurement of (1) the lifetimes of hypernuclei, (2) the branching ratios of π^{-} mesonic decay and proton-induced nonmesonic decay, and (3) to obtain the energy spectra of the protons from nonmesonic decay. In this paper, the results for lifetimes will be presented, which may show the mass dependence of the hypernuclear lifetime. The lifetimes of the ground state of ${}^{12}_{\Lambda}$C, ${}^{28}_{\Lambda}$Si, and the bound region of ${}^{56}_{\Lambda}$Fe have been reported [24].

In Sec. II, the details of the experimental apparatus will be presented. Section III will show the analysis procedures and the lifetime results. In Sec. III, the systematic uncertainties of the present results also will be considered. We will compare the present measurements with previous results and the theoretical calculations in Sec. IV.

II. EXPERIMENT

Λ hypernuclei were produced via the (π^{+},K^{+}) reaction. The lifetimes of the Λ hypernuclear weak decay were extracted from the distribution of the time differences between beam injection and the emission of protons from the hypernuclear weak decay.

The (π^{+},K^{+}) reaction is suitable for measuring the weak

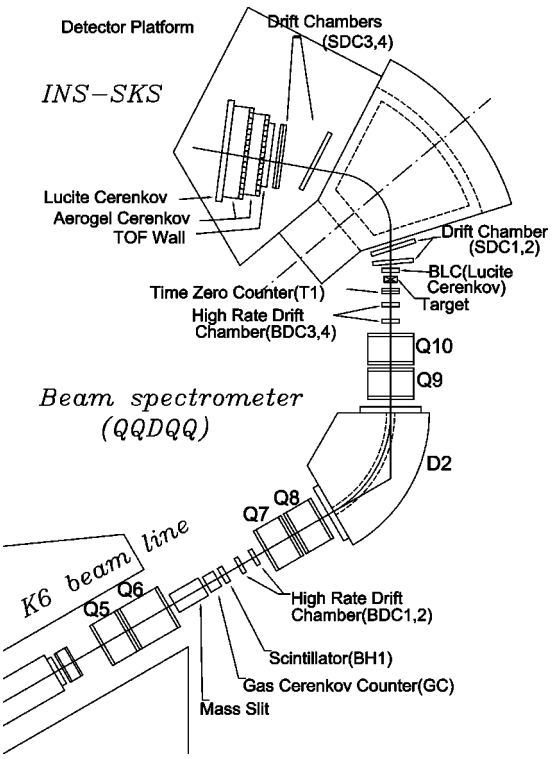

FIG. 1. Schematic view of the K6 beam line of KEK-12 GeV PS and the superconducting kaon spectrometer (SKS).

decay of medium and heavy Λ hypernuclei because it can produce the deeply bound state of hypernuclei due to the high momentum transfer which is as much as 0.4 GeV/c, while the (K^-,π^-) reaction populates preferentially the substitutional states due to the reaction selectivity. In addition, the (π^+,K^+) reaction gives a very clean inclusive spectrum because it is free from the decay of beam particles. This permits us to estimate the yield of hypernuclear formation in the inclusive spectrum rather precisely.

A. General description

The Λ hypernuclei were produced via the (π^+,K^+) reaction using the 1.05 GeV/c π^+ beam at the K6 beam line [25] of the KEK 12-GeV PS. The scattered kaons were tagged using a superconducting kaon spectrometer (SKS) [26] to identify the production of hypernuclei and reconstruct the hypernuclear mass spectrum.

Figure 1 shows a schematic view of the beam line spectrometer and the scattered particle spectrometer (SKS). The acceptance of the SKS is about 100 mSr and a good momentum resolution of 0.1% full width at half maximum (FWHM) was achieved at the previous experiment (KEK-PS E140a) for the hypernuclear spectroscopy [26,27].

We used natural carbon, silicon, and iron as a target. We placed targets at finite angles to the beam as shown in Fig. 2. The reason for this asymmetric configuration is as follows: (a) in order to increase the effective target thickness for the beam to generate a larger hypernuclear production rate and (b) in order to decrease the path length of the decay products in the target material. This will reduce the detection threshold and the deterioration of the energy distribution. The tilt angle for the target was about 10°, giving a target about 5 times thicker for the beam than for the decay products. In Table II, the specifications for each target are summarized.

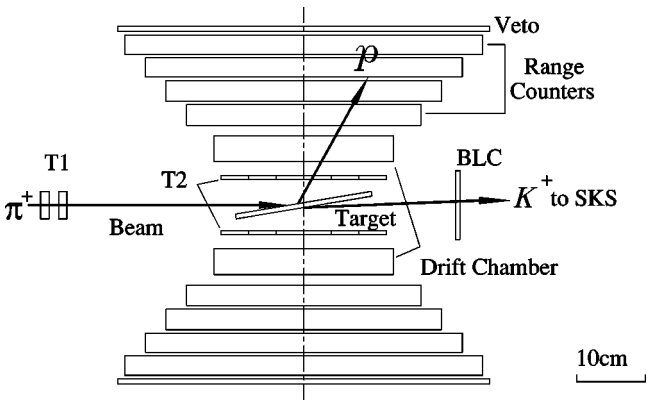

FIG. 2. Schematic view of the coincidence detector system used in the lifetime measurement of hypernuclei. The superconducting kaon spectrometer (SKS) is not shown and is located farther to the right.

Each run typically lasted 2 h and the beam spill was about 1.7 s out of every 4 s. The typical beam intensity was about 3.7×10^6 pions/spill. The (π^+,K^+) event rate at the trigger level was about 400/spill and most of these events were related to the background (π^+,π^+) or (π^+,p) events.

B. Coincidence part: For the detection of the weak decay

The charged decay products of the hypernucleus were detected by the coincidence detector system which consists of fast timing counters, range counters, and drift chambers. The acceptance was estimated to be about 30% by GEANT-[29] based Monte Carlo simulation and the detection threshold was about 30 MeV for protons and 12 MeV for negative pions. Figure 2 shows a schematic view of the coincidence detector system which is located symmetrically above and below the target. Table III shows the specifications of each detector.

The first element (T2) is the fast timing counter which determines the timing of charged decay products. T2 is divided into six segments of plastic scintillator with $4[\mathrm{W}]\times18[\mathrm{L}]\times0.6[\mathrm{T}]\ \mathrm{cm}^3$ with double-sided readout. The intrinsic time resolution of each segment is about 37 ps for a 100 MeV proton and about 70 ps for minimum ionizing particles obtained from a separate test experiment [30] after time walk correction. The dE/dx information given by the T2 counter was used for particle identification.

TABLE II. The specifications of experimental targets.

Target	Thickness ($\mathrm{g/cm^2}$)	Abundance (%)	N_{beam} ($\times10^9$)
^{12}C	6.45	98.89 (natural)	272
^{28}Si	10.35	92.23 (natural)	1470
^{56}Fe	7.00	91.80 (natural)	959

TABLE III. The specifications of the coincidence detectors.

	Active area (cm^2)	Thickness (cm)	
T1	8×9.6	1.2	Two layers of four segments
T2	24×18	0.6	Six segments (4 cm wide)
RG1	34×34	2.4	Six layers (0.4 cm thick)
RG2	40×40	2.4	Six layers (0.4 cm thick)
RG3	46×46	2.4	Four layers (0.6 cm thick)
RG4	52×52	2.4	Four layers (0.6 cm thick)
VETO	54×54	0.4	—
PDC	26×26	4 mm[a]	Six planes ($XX'YY'XX'$)
	δt (FWHM)	200 ps	
	$E_{threshold}$	30 MeV for proton, 12 MeV for π^-	
	Acceptance	30%	

[a]Drift distance.

The next element [multiwire drift chamber (PDC)] is the multiwire drift chamber which has six planes ($XX'YY'XX'$), where X is along the beam direction and Y is perpendicular to the beam direction. Each plane has a 4 mm drift distance and the anode wires of the primed planes are shifted by half a cell size (4 mm) to resolve left/right ambiguity. The PDC gives the tracks of the decay particles. The reaction point of hypernuclear production was determined by the beam line spectrometer and SKS. Since the recoil velocity of a hypernucleus is very small, we can assume that the decay of the produced hypernucleus occurs at its production vertex. However, the spatial resolution of the production vertex along the beam direction was as low as a few cm and the decay vertex was estimated by the intersection of the tracks of a decay particle and beam.

The third element is the range counter. The range counter is divided into four sets. The first two sets ($RG1,2$) consist of six layers each 4 mm thick and the other two sets ($RG3,4$) consist of four layers each of 6-mm-thick plastic scintillator. The total thickness of the range counter block is 9.6 cm. The range of the decay particle ($RANGE$) was determined by the path length in the range counter after the incident angle correction. The energy of the incident particle was calculated from the range after the particle was identified.

The last element (VETO) is to veto the charged particles which pass through the whole set of the range counter.

The particle identification has been done using dE/dx-$RANGE$ and dE/dx-E relations. dE/dx was defined as the energy deposit in the T2 counter in unit length. $RANGE$ is the path length in the coincidence detectors and E was defined as the total energy deposit digitized by analog-to-digital converters (ADC's) measured in T2 and the range counter:

$$PID_1 = \ln\frac{dE}{dx} + f_1(\ln RANGE), \tag{7}$$

$$PID_2 = \frac{dE}{dx} + f_2(E), \tag{8}$$

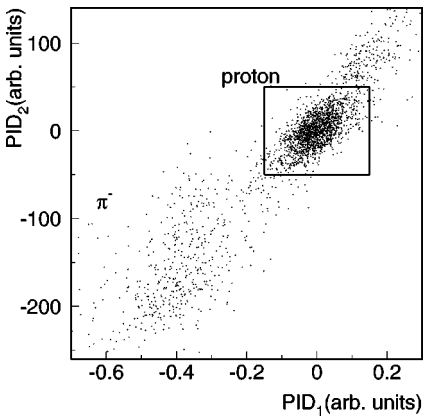

FIG. 3. The scatter plot of two PID functions. The x axis is the PID_1 using dE/dx and $RANGE$ and the y axis the PID_2 using dE/dx and E. The events inside the box were accepted as protons.

where f_1 and f_2 are the first order polynomials. Figure 3 shows the scatter plot of PID_1 and PID_2 for the hypernuclear bound state events. The events inside the box were accepted as protons for the lifetime analysis. Figure 4 shows the projection of PID_1. The shaded section represents the events remaining after applying the PID_2 cut and the events between the two arrows were accepted as protons. From the figure, the pion fraction in the proton gate is estimated to be less than 2%.

C. Fast timing measurement system

The hypernuclear lifetime is the mean value of the differences between the production time (t_p) and the decay time (t_d) of the hypernuclei ($\Delta t = t_d - t_p$). The production time (t_p) was extracted from the beam timing (t_1) and the flight time (t_{f_b}) of the beam from the beam timing counter (T1) to the production vertex ($t_p = t_1 + t_{f_b}$). The decay time (t_d) was determined by subtracting the timing (t_2) of decay products at the T2 counter and the flight time (t_{f_d}) from the decay vertex to the T2 counter ($t_d = t_2 - t_{f_d}$). The time resolution is

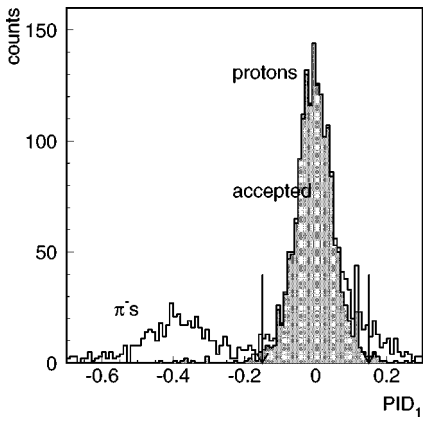

FIG. 4. Particle identification plot (PID_1) using dE/dx and $RANGE$ shows proton and pion peaks. The shaded region represents the events after PID_2(dE/dx vs E) cut. The events of the shaded region between the two arrows are accepted as protons.

due to four terms: $\sigma=\sqrt{\sigma_{t_2}^2+\sigma_{t_{f_d}}^2+\sigma_{t_1}^2+\sigma_{t_{f_p}}^2}$. The two terms related to the flight time are predominantly determined by the geometry of the timing counter system (flight length) and the others are the intrinsic resolutions of the timing counters ($\sigma_{t_{1,2}}$). The contribution from each term is estimated to be about 70–94 ps in FWHM.

Since we used the leading-edge discriminator, a correction due to the time walk effect was essential to achieve a high time resolution. We corrected for the time walk effect using the relation $\delta t\sim(1/\sqrt{q}-1/\sqrt{q_0})$, where δt is the amount of correction, and q and q_0 the integrated charge in the ADC and its mean value [31].

The beam timing was determined by T1 which consists of two layers (T11 and T12) of plastic scintillators (see Fig. 2). Each layer of T1 is segmented into 4 with a size of $8[\mathrm{L}]\times 1.3(3.5)[\mathrm{W}]\times 1.2[\mathrm{T}]\ \mathrm{cm}^3$ for the center (side) two segments. The center segments have a smaller width because of the beam profile thus making the beam intensity about $0.4\times10^6\pi^+$'s/s for the side segments and about $0.65\times10^6\pi^+$'s/s for the center ones. Each segment has photomultiplier tubes (PMTs) on both ends and a three-stage booster in a high voltage chain is used to avoid the nonlinearity of PMTs at high beam rates. We constructed T1 from two layers of 1.2 cm thickness because the improvement in the time resolution due to the number of scintillating photons ($N_{p.e.}$) for the minimum ionizing particle seems to saturate like $\sigma\propto\sqrt{1/N_{p.e.}}$ at a scintillator of 1.2 cm thickness.

The intrinsic time resolution (FWHM) of T1 counter is about 108 ps for the center segments and about 127 ps for the side segments at a beam intensity of $2\times10^6\pi^+$'s/s after time walk correction and it is about 50% worse than the low rate incidence [30]. For beam timing, we used the average of the timings of two layers and the beam time resolution (σ_{t_1}) is about 82 ps in FWHM.

The timing of decay products was determined by T2 and was described in Sec. II B.

D. Time response function of the system

In order to obtain the time response function of the system, we used prompt events from the (π^+,pp) reaction which results from the strong interaction.

The Δt distribution of the (π^+,pp) events — the prompt time spectrum — was used for the time response function of the system. Since most events identified as kaons in the trigger level were protons or pions, we could collect plenty of (π^+,pp) events simultaneously with hypernuclear weak decay events. The recoiled proton was tagged by SKS and the other proton was detected and analyzed by coincidence detectors. Since the (π^+,pp) reaction is a strong interaction, the (π^+,pp) events could give a prompt response.

Since the timing counters are segmented into 8 (T1) or 12 (T2), it is essential to match the relative timing of each segment. In addition, as the experiment was performed over a period of 1 yr, the time drift due to the temperature or other environmental changes during the experiment should be considered. The long-term time drift was typically a few tens of picoseconds and at most about 200 ps. All these effects were corrected using the prompt time spectrum of the (π^+,pp) events. The relative timings of T1 (8 segments) and T2 (12 segments) was matched mostly every 4 h. Figure 5 shows the typical prompt time spectrum, the resolution of which is 200 ps FWHM.

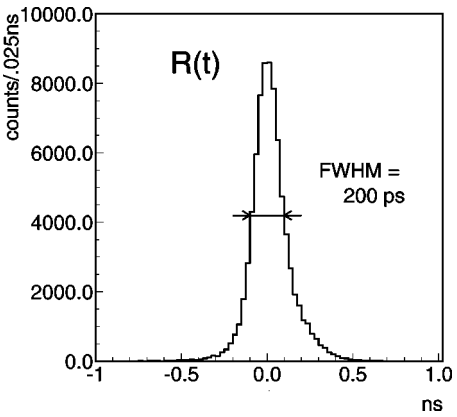

FIG. 5. The time response function of the system which is obtained using the prompt (π^+,pp) events. The total resolution is 200 ps FWHM (85 ps in σ).

III. ANALYSIS AND RESULTS

A. Singles spectra

Figure 6 shows the reconstructed hypernuclear mass spectra of ${}^{12}_{\Lambda}\mathrm{C}$: (a) inclusive, (b) in coincidence with energetic protons, and (c) with the pions from the hypernuclear decay. The inclusive spectrum shows a constant background level of about 43 events per 1 MeV but the coincidence spectra are

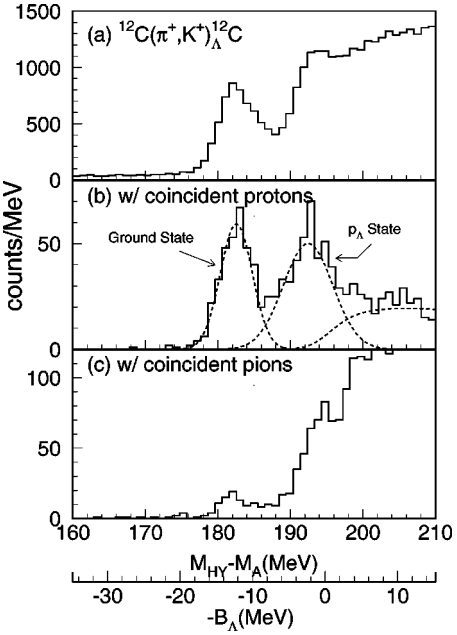

FIG. 6. The hypernuclear mass spectra for ${}^{12}_{\Lambda}\mathrm{C}$, (a) inclusive, (b) in coincidence with protons, and (c) in coincidence with pions. $M_{HY}-M_A$ means the mass difference between a Λ hypernucleus and a target nucleus. B_Λ is the binding energy of a Λ hyperon.

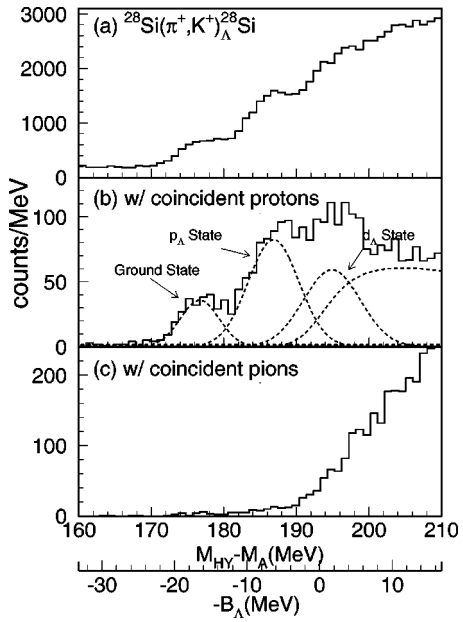

FIG. 7. The hypernuclear mass spectra for $^{28}_{\Lambda}$Si, (a) inclusive, (b) in coincidence with protons, and (c) in coincidence with pions. $M_{HY}-M_A$ means the mass difference between a Λ hypernucleus and a target nucleus. B_Λ is the binding energy of a Λ hyperon.

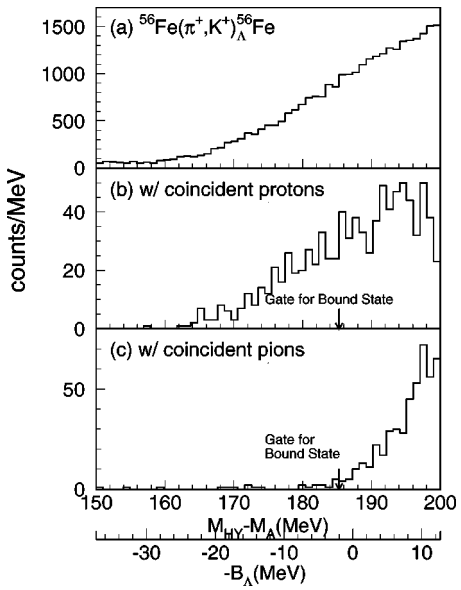

FIG. 8. The hypernuclear mass spectra for $^{56}_{\Lambda}$Fe, (a) inclusive, (b) in coincidence with protons, and (c) in coincidence with pions. $M_{HY}-M_A$ means the mass difference between a Λ hypernucleus and a target nucleus. B_Λ is the binding energy of a Λ hyperon.

almost background free. The *x* axis indicates the mass difference between a hypernucleus (M_{HY}) and a target nucleus (M_A). The Λ binding energy (B_Λ) is also shown. The absolute scale of the spectra was adjusted so that the Λ binding energy of the ground state of $^{12}_{\Lambda}$C was 10.8 MeV [27]. The proton coincidence spectrum shows two clear peaks at $M_{HY}-M_A=184$ MeV ($B_\Lambda=11$ MeV) and 194 MeV (0 MeV) which are well-known states with a neutron-hole Λ-particle configuration of $[0p_{3/2}^{-1}s_\Lambda]$ and $[0p_{3/2}^{-1}p_\Lambda]$ of $^{12}_{\Lambda}$C, respectively. The core-excited states of ^{11}C with the Λ hyperon in the s_Λ orbit [28] could not be resolved due to the limited resolution. The p_Λ state was a particle unbound state and it is known to decay through proton emission to the lighter $^{11}_{\Lambda}$B hypernucleus [32].

For the $^{28}_{\Lambda}$Si hypernucleus, the measurements were done in two separated beam cycles; one was run in February 1995 and the other in July 1995. Both cycles showed consistent hypernuclear mass spectra. Figure 7 shows the mass spectra collected in February 1995. The inclusive spectrum (a) shows a constant background level of about 160 events per 1 MeV and the peak structure is not clean. The mass spectrum in coincidence with the energetic protons (b) shows three peaks at $M_{HY}-M_A\simeq178$ MeV ($B_\Lambda\simeq17$ MeV), $\simeq188$ MeV ($\simeq5$ MeV), and $\simeq195$ MeV ($\simeq-12$ MeV) with a much smaller background level. Again, as a result of the limited resolution of the spectrum, the whole structure of $^{28}_{\Lambda}$Si could not be resolved [27,33]. Figure 7 in Ref. [27] shows four clear peaks in the Λ bound region and the whole mass spectrum of $^{28}_{\Lambda}$Si was fitted with five Gaussians. In this analysis, as shown in Fig. 7(b), the fitting was done with three Gaussian functions, considering the first two peaks of Fig. 7 in Ref. [27] as one peak and the next two peaks as another peak. However, the configuration of each peak could be assigned as s_Λ, p_Λ, and d_Λ states, following Ref. [27]. The s_Λ state is the ground state of $^{28}_{\Lambda}$Si and the p_Λ state decays through proton emission to the lighter hypernucleus of $^{27}_{\Lambda}$Al because the proton emission threshold is at $B_\Lambda\simeq9$ MeV. Neutron emission is forbidden because of the negative reaction *Q* value. The d_Λ state is above the Λ emission threshold ($B_\Lambda=0$ MeV).

Figure 8 shows the mass spectra of $^{56}_{\Lambda}$Fe: (a) inclusive, (b) in coincidence with the energetic protons, and (c) with the pions from the hypernuclear decay. The inclusive spectrum shows a constant background level of about 50 events per 1 MeV but the background level of the coincidence spectra is negligible. The spectra in coincidence with protons and pions show that the region of $M_{HY}-M_A<187$ MeV corresponds to the Λ bound state. In this case, the hypernuclear mass spectrum in coincidence with energetic protons corresponds to $^{56}_{\Lambda}$Fe states but the coincident protons come not only from $^{56}_{\Lambda}$Fe states but also from the lighter hypernuclei which are produced through particle emission. From a simple estimate using the reaction *Q* value and Coulomb barrier, the residual hypernuclei after particle emission can be $^{55}_{\Lambda}$Fe or $^{55}_{\Lambda}$Mn. From now on, for convenience, $_{\Lambda}$Fe will be used to represent all those hypernuclei including $^{56}_{\Lambda}$Fe.

B. Lifetime measurements

The hypernuclear decay rate should follow the probability distribution

$$P(t)=\frac{1}{\tau}e^{-t/\tau}, \tag{9}$$

where τ is the mean life of a hypernucleus and $P(t)$ is the decay rate at time *t*. Since the measurement has a finite reso-

lution, the actual time distribution $S(t)$ is the convolution of $P(t)$ with the response function $R(t)$ of the detector system,

$$S(t)=\int_0^\infty P(t')R(t-t')dt'. \tag{10}$$

To zeroth order, the lifetime of the hypernucleus can be determined by the mean difference between the prompt time spectrum and the time spectrum of hypernuclear weak decay which would be delayed due to the hypernuclear lifetime (the delayed time spectrum). Figure 9 shows the comparison of prompt and delayed time spectra for (a) the ground state of ${}^{12}_{\Lambda}$C, (b) the ground state of ${}^{28}_{\Lambda}$Si, and (c) the whole Λ bound region of ${}^{56}_{\Lambda}$Fe, where the spectrum for ${}^{28}_{\Lambda}$Si contains data taken at the February run (only half of the whole data). The differences of the mean values of prompt and delayed time spectra are 237, 205, and 219 ps, respectively. The time spectrum for each target contains 324, 281, and 428 events for the delayed spectrum and 1.7×10^4, 7.8×10^4, and 1.9×10^4 events for the prompt spectrum.

The lifetime was extracted by fitting the delayed time spectra of hypernuclear decay events with the function $S(t)$, considering the lifetime as a free fitting parameter. The fitting was performed with the maximum likelihood fitting method adopting Poisson statistics for each measurement which has been shown to produce fewer fitting errors than the normal least squares method [34]. As a response function, we used the prompt time spectra themselves from

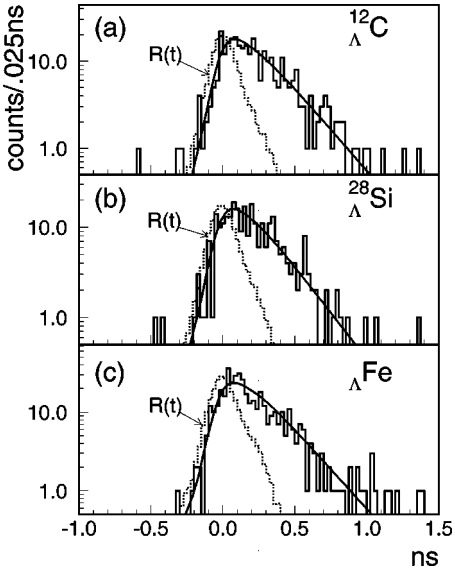

FIG. 9. The prompt and the delayed time spectra are compared for (a) the ground-state region of ${}^{12}_{\Lambda}$C, (b) the ground-state region of ${}^{28}_{\Lambda}$Si, and (c) the whole bound region of ${}^{56}_{\Lambda}$Fe.

(π^+,pp) events which were obtained simultaneously with those of the hypernuclear production (see Sec. II C). The solid curves in Fig. 9 show the fitting results and the reduced chi squares (χ^2/ν) of the fits are 0.67 for ${}^{12}_{\Lambda}$C, 0.90 for ${}^{28}_{\Lambda}$Si, and 0.79 for ${}_{\Lambda}$Fe.

The results of maximum likelihood fitting (τ_{FIT}) are

$$\begin{aligned}
\tau_{FIT} &= 230^{+15}_{-14} \text{ ps (with 324 events for the ground state region of } {}^{12}_{\Lambda}\text{C)},\\
&= 211^{+12}_{-12} \text{ ps (with 263 events for the } p_\Lambda \text{ state region of } {}^{12}_{\Lambda}\text{C)},\\
&= 206^{+11}_{-10} \text{ ps (with 528 events for the ground state region of } {}^{28}_{\Lambda}\text{Si)},\\
&= 204^{+10}_{-10} \text{ ps (with 837 events for the } p_\Lambda \text{ state region of } {}^{28}_{\Lambda}\text{Si)},\\
&= 215^{+14}_{-13} \text{ ps (with 428 events for the Λ bound region of } {}^{56}_{\Lambda}\text{Fe)},
\end{aligned}$$

where the quoted errors correspond to one standard deviation (68% confidence level) and are only statistical. For the lifetime analysis of ${}^{28}_{\Lambda}$Si, the lifetime was obtained independently for two separate data sets and the final lifetime of ${}^{28}_{\Lambda}$Si was obtained by averaging over the two fitting values. The values for ${}^{28}_{\Lambda}$Si were the averaged (or summed) values over all the silicon data. In the case of ${}^{56}_{\Lambda}$Fe, the value is the average of those of ${}^{55}_{\Lambda}$Mn, ${}^{55}_{\Lambda}$Fe, and ${}^{56}_{\Lambda}$Fe. The event sample for each hypernuclear state was selected with the gate condition shown in Table IV. The asymmetric gate condition is applied in order to reduce the fraction of other states of Λ as much as possible. The simplified fitting mentioned in Sec. III tells us that the fraction of other states is at most 13%. However, the estimation of the fraction depends on the fitting method for the hypernuclear mass spectra. When the fitting was done using all the peaks known from the other experiment [27], the fraction of other states reaches as high as 20%.

TABLE IV. The gate condition for each hypernuclear single-particle state and the fraction of the various states.

	Gate window $M_{HY}-M_A$(MeV)	Number of events	1s state	1p state	Higher states
${}^{12}_{\Lambda}$C	175–186 (1s gate)	323	97%	3%	0%
	188–197 (1p gate)	338	1%	93%	6%
${}^{28}_{\Lambda}$Si	171–181 (1s gate)	527	87%	13%	0%
	183–188 (1p gate)	661	1%	94%	5%
${}_{\Lambda}$Fe	160–185 (bound states)	309	—	—	—

C. Systematic uncertainties of lifetime measurements

1. Contribution from the response function

Since the prompt time spectrum of the (π^+,pp) events was used as the time response function of the system, the lifetime analysis of hypernuclear weak decay mainly depends on the analysis of (π^+,pp) events.

The prompt time spectrum is expected to follow a Gaussian distribution, whose mean is at $t=0$ and whose standard deviation corresponds to the time resolution of the detector system. However, as shown in Fig. 5, the prompt time spectrum has a non-Gaussian component, predominantly in the delayed time region.

In order to investigate the source of the non-Gaussian component, we checked the time of flight of the beam. The time of flight of the beam particles (TOF_{beam}) is determined by $TOF_{beam}=t_1-t_0$, where t_1 is the timing at the T1 counter located at the target area and t_0 is the timing at the BH1 counter in the most upstream section of the beam line (see Fig. 1). The TOF_{beam} distribution also shows a non-Gaussian shape and the non-Gaussian component of the prompt time spectrum was strongly correlated with that of TOF_{beam}. Most of the non-Gaussian component in the prompt spectrum came from the events of $TOF_{beam}<0$ and the prompt time spectrum becomes a Gaussian shape for the events of $TOF_{beam}>0$. The TOF_{beam} spectrum of (π^+,pp) events and that of the hypernuclear decay events showed almost the same distribution. We compared the fitting results for the events of $TOF_{beam}>0$ and those of $TOF_{beam}<0$. The results of the fitting to the two separate data sets agree well with each other to within statistical fluctuations.

The timing offset should also be the same for both events because the difference in timing offsets directly affects the final lifetimes. In order to confirm this point, we set the difference in timing offsets as a fitting parameter and performed the maximum likelihood fitting. The fitting function was

$$S'(t)=\int_0^\infty \frac{1}{\tau} e^{-t'/\tau} R(t-t'+t_0)dt', \tag{11}$$

where t_0 as well as τ was a fitting parameter. In order to avoid the histogram binning effect, the step size in the variation of t_0 was fixed to 25 ps. The fitting shows that χ^2 was minimized for all sets of data at $t_0=0$. We conclude that the timing offset of the prompt spectrum and the delayed spectrum should be same.

From the above investigations, we conclude that no systematic differences in the time response of the detector system for (π^+,pp) and hypernuclear decay events were observable and that the systematic uncertainties of the lifetime due to the (π^+,pp) events are negligible compared to the statistical uncertainties.

2. Other considerations

We investigated the other systematics, e.g., the independent lifetime analysis for up- and down-coincidence detector systems, the dependence of decay proton energy, and the beam momentum dependence of lifetimes. The fluctuations shown in these analyses are within statistical ranges. In addition, since we used the time difference of two distributions (the prompt and the delayed time spectra) which were measured at the same time, most of the instrumental errors such as errors in the relative positions of timing counters would be canceled out.

TABLE V. The summary of lifetime measurements. The value for ${}_\Lambda$Fe represents the average lifetime of ${}^{55}_\Lambda$Mn, ${}^{55}_\Lambda$Fe, and ${}^{56}_\Lambda$Fe.

	Number of events	Lifetime (ps)	Γ (Γ_Λ)
${}^{12}_\Lambda$C	323	231 ± 15	1.14 ± 0.08
${}^{11}_\Lambda$B	338	211 ± 13	1.25 ± 0.08
${}^{28}_\Lambda$Si	527	206 ± 12	1.28 ± 0.08
${}^{27}_\Lambda$Al	661	203 ± 10	1.30 ± 0.07
${}_\Lambda$Fe	309	215 ± 14	1.22 ± 0.08

Since the resolution of the hypernuclear mass spectra is limited due to the use of a thick target, each state of Λ could not be well separated and the fraction of other states in the gate for the various Λ single-particle states should be considered. From the chi-square fitting of hypernuclear mass spectra for ${}^{12}_\Lambda$C and ${}^{28}_\Lambda$Si, the fraction of the various Λ states was estimated as shown in Table IV. The effect of other states should be small, not only because the fraction of other states was small, being at most $\sim$ 10%, but also because the fitting results of each gate are not so different from each other (less than 10%).

The correction was made by solving following simultaneous equations, with the assumption that the fitting value of higher states (h.s.) (see Table IV) is affected only by the lower states:

$$\tau_1=\tilde{\tau}_{1s}w_{11}+\tilde{\tau}_{1p}w_{12}+\tilde{\tau}_{h.s.}w_{13},$$

$$\tau_2=\tilde{\tau}_{1s}w_{21}+\tilde{\tau}_{1p}w_{22}+\tilde{\tau}_{h.s.}w_{23},$$

$$\tau_3=\tilde{\tau}_{1s}w_{31}+\tilde{\tau}_{1p}w_{32}+\tilde{\tau}_{h.s.}w_{33},$$

where τ_i is the fitting result for each ith gate, $\tilde{\tau}_j$, where j is $1s$, $1p$, or h.s., is the real lifetime of each state, and w_{ij} is the weighting of the jth state ($1s$, $1p$, h.s.) to the ith gated region listed in Table IV. Table V shows the results of the corrections. As expected, the correction is much smaller than the statistical uncertainty.

In conclusion, we cannot find any systematics comparable to the statistical uncertainties. The experimental error level was predominantly determined by the statistical errors.

IV. DISCUSSION

A. Comparison with the previous experimental results

In Table VI, the present lifetime results are compared with the earlier measurements. The lifetimes of ${}^{12}_\Lambda$C and ${}^{11}_\Lambda$B are consistent with the previous measurements of Grace *et al.* [17] with much lower uncertainties. The previous ${}^{12}_\Lambda$C lifetime measurement was done with the K^- beam at BNL-

TABLE VI. The comparison with the previous measurements. The value for ${}_{\Lambda}$Fe represents for the average lifetime of ${}^{55}_{\Lambda}$Mn, ${}^{55}_{\Lambda}$Fe, and ${}^{56}_{\Lambda}$Fe.

	Present results (ps)	Previous measurement (ps)
${}^{11}_{\Lambda}$B	211 ± 13	192 ± 22 [17,16]
${}^{12}_{\Lambda}$C	231 ± 15	211 ± 31 [17,16]
${}^{\sim 16}_{\Lambda}$Z	—	86^{+33}_{-26} [18]
${}^{27}_{\Lambda}$Al	203 ± 10	—
${}^{28}_{\Lambda}$Si	206 ± 12	—
${}_{\Lambda}$Fe	215 ± 14	—

AGS. It produced a hypernucleus using the (K^-,π^-) reaction and tagged pions to identify the hypernuclear production. The hypernuclear mass spectrum was reconstructed.

The only earlier measurement in the medium mass region for nuclei heavier than ${}^{12}_{\Lambda}$C is the lifetime of $A\sim16$ hypernuclei (${}^{\sim 16}_{\Lambda}$Z) measured by Nield *et al.* [18]. They used a 2.1 GeV/nucleon ^{16}O beam at the Lowrence Berkeley Laboratory (LBL) Bevalac and a polyethylene target. The production of low momentum K^+ mesons and their delayed decay after stopping were used as the trigger for the hypernuclear production. They could not reconstruct the hypernuclear mass spectrum and identify the hypernuclear species. They extracted the lifetime from the recoil distance distribution which was measured by spark chambers. They had a lot of background events which came from the interaction with the Al window of the spark chamber and also the trigger counter at downstream of the target. After the subtraction of the large background, the remaining events constituted only 22 events and the lifetime from the maximum likelihood fitting of the recoil distance distribution was $\tau=86^{+33}_{-26}$ ps, which is much smaller than the lifetime of ${}^{12}_{\Lambda}$C and ${}^{28}_{\Lambda}$Si.

B. Comparison with the calculations

Up to now, three groups have presented the calculations for lifetimes of various Λ hypernuclei. First, in 1985, Oset and Salcedo [35] made lifetime calculations using Λ self-energies for nuclear matter. They included only one-pion exchange for the nonmesonic decay which governs the hypernuclear weak decay for the medium and heavy mass regions. In order to apply their calculation to the finite hypernuclei, they used the local-density approximation and obtained the lifetimes of ${}^{5}_{\Lambda}$He to ${}^{208}_{\Lambda}$Pb. Their calculations give much shorter lifetimes than the measurements with values about 60–70 % of the measurements.

Ramos *et al.* [36] calculated the lifetimes in 1994 based on Oset and Salcedo's calculation. They used a one-pion exchange model including the two-nucleon-induced decay mode ($\Lambda NN\rightarrow NNN$). In $\Lambda NN\rightarrow NNN$, the strongly correlated two nucleons (mainly proton-neutron pair) and Λ exchange a virtual pion. They gave the lifetimes for medium and heavy hypernuclei (from ${}^{12}_{\Lambda}$C to ${}^{208}_{\Lambda}$Pb). Their calculation also gave similar values to Oset and Salcedo's, which were about 60–70% of the measurement values. However, the calculations of Ramos *et al.* yield slightly shorter values than Oset and Salcedo's.

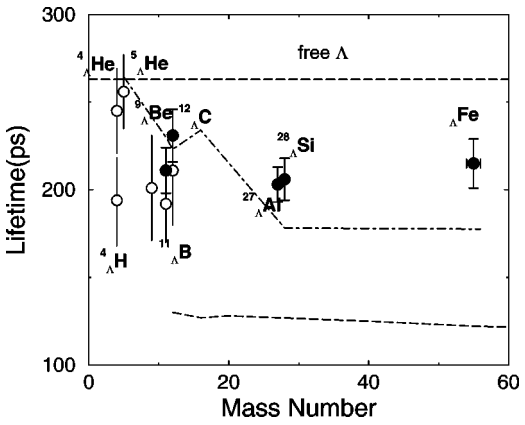

FIG. 10. The mass dependence of hypernuclear lifetimes. The open circles represent the data from the previous counter experiments and the solid circles the present results. The dot-dashed line shows the calculations by Itonaga *et al.* and the dashed line shows the calculations by Ramos *et al.*

Recently, Itonaga *et al.* calculated the hypernuclear lifetime by adopting a one-pion and $2\pi/\rho$, $2\pi/\sigma$ exchange potential for nonmesonic decay, including *p*-shell nucleons as well as *s*-shell nucleons [37]. They gave the lifetimes of ${}^{5}_{\Lambda}$He, ${}^{12}_{\Lambda}$C, ${}^{28}_{\Lambda}$Si, and ${}^{56}_{\Lambda}$Fe. Their calculation reproduced the Λ hypernuclear lifetimes quite well even though they gave slightly shorter values for ${}^{28}_{\Lambda}$Si and ${}^{56}_{\Lambda}$Fe.

C. Lifetimes for the overall hypernuclear mass region

Figure 10 shows the hypernuclear lifetimes for the overall hypernuclear mass region. The solid circles are the present results and the open circles are the results from previous counter experiments with explicit identifications of the generated Λ hypernuclei. The horizontal error bars for the ${}_{\Lambda}$Fe data represents the mass range of the hypernuclei. The hypernuclear lifetimes are shorter than the free Λ lifetime except for the very light hypernuclei and are almost constant at about 80% of the free Λ value in the hypernuclear mass region of $A\gtrsim12$. The lifetimes of ${}^{28}_{\Lambda}$Si and ${}_{\Lambda}$Fe are slightly shorter than that of ${}^{12}_{\Lambda}$C. However, the differences are within experimental uncertainties.

The theoretical calculations are overlaid indicated by the dash-dotted line (the calculation of Itonaga *et al.*) [37] and the dashed line (Ramos *et al.*) [36] in Fig. 10. The calculations of Ramos *et al.* show that the lifetime does not change very much according to the hypernuclear mass number. However, their mass number dependence reflects only the overlap area of the wave functions of the Λ and nucleon because they used the local-density approximation. The calculations of Itonaga *et al.* also show a saturation of lifetimes but the effect seems to be a little weaker than for the measurements. This may indicate that their 2π exchange potential has a longer range than the actual one.

V. CONCLUSION

We have measured the lifetimes of ${}^{11}_{\Lambda}$B, ${}^{12}_{\Lambda}$C, ${}^{27}_{\Lambda}$Al, ${}^{28}_{\Lambda}$Si, and ${}_{\Lambda}$Fe hypernuclei. For the hypernuclei with $A>12$ which

are in the mass range beyond the *p*-shell hypernuclei this is the first measurement which can explicitly identify the Λ hypernuclear bound states.

The present results together with the previous measurements show that the lifetimes are almost constant at about 80% of the free Λ value in the hypernuclear mass region above $A=12$. This weak mass dependence should be related to the mechanism of nonmesonic decay, which is dominant in the present mass region, and to the baryon-baryon short range correlation inside the hypernucleus.

Assuming the short range nature of the nonmesonic weak decay process, one can employ a zero range approximation for a qualitative understanding. The nonmesonic weak decay widths will then be proportional to the overlap integral of the wave functions of a nucleon and a Λ, and the hypernuclear lifetimes will be almost constant in the mass region beyond carbon where the overlap integrals almost saturate. A simple discussion of the weak mass dependence was also made recently by assuming a sufficiently short range interaction and by counting the number of ΛN bonds responsible for the nonmesonic weak decay [38].

The present lifetime data apparently require us to take into account the short range nature of the nonmesonic weak decay, which does not seem to be properly incorporated in the current meson exchange model.

ACKNOWLEDGMENTS

We are grateful for the generous support from the staff members of KEK and the old INS. We also deeply appreciate the continuous encouragement by Professor K. Nakai and Professor T. Yamazaki throughout this experiment from the beginning. We very much benefited from discussions with Professor Itonaga, Professor T. Motoba, Professor T. Fukuda, and Professor T. Nagae. H.B. acknowledges partial support from the Korea-Japan collaborative research program of KOSEF and from the Ministry of Education through the Research Institute of Basic Science of Seoul National University.

[1] Particle Data Group, C. Caso *et al.*, Eur. Phys. J. C **3**, 673 (1998).
[2] J. Cohen, Prog. Part. Nucl. Phys. **25**, 139 (1990).
[3] W. M. Alberico, A. De Pace, M. Ericson, and A. Molinari, Phys. Lett. B **256**, 134 (1991).
[4] E. G. Adelberger and W. Haxton, Annu. Rev. Nucl. Part. Sci. **35**, 501 (1985).
[5] J. Haidenbauer, K. Holinde, K. Kilian, T. Sefzick, and A. W. Tomas, Phys. Rev. C **52**, 3496 (1995).
[6] R. J. Prem and P. H. Steinberg, Phys. Rev. **136**, B1803 (1964).
[7] R. E. Phillips and J. Schneps, Phys. Rev. **180**, 1307 (1969).
[8] G. Bohm, J. Klabuch, U. Krecker, and F. Wysotzki, Nucl. Phys. **B16**, 46 (1970).
[9] G. Keyes, M. Derrick, T. Fields, L. G. Hyman, J. G. Fetkovich, J. McKenzie, B. Riley, and I.-T. Wang, Phys. Rev. D **1**, 66 (1970).
[10] G. Keyes, J. Sacton, J. H. Wickens, and M. M. Block, Nucl. Phys. **B67**, 269 (1973).
[11] Y. W. Kang, N. Kwak, J. Schneps, and P. A. Smith, Phys. Rev. **139**, B401 (1965).
[12] H. Outa, M. Aoki, R. S. Hayano, T. Ishikawa, M. Iwasaki, A. Sakaguchi, E. Takada, H. Tamura, and T. Yamazaki, Nucl. Phys. **A585**, 109c (1995).
[13] H. Outa, M. Aoki, R. S. Hayano, T. Ishikawa, M. Iwasaki, A. Sakaguchi, E. Takada, H. Tamura, and T. Yamazaki, Nucl. Phys. **A639**, 251c (1998).
[14] V. J. Zeps, Nucl. Phys. **A639**, 261c (1998).
[15] G. Bohm, J. Klabuhn, U. Krecker, F. Wysotzki, G. Bertrand-Coremans, J. Sacton, J. Wickens, D. H. Davis, J. E. Allen, and K. Garbowska-Pniewska, Nucl. Phys. **B23**, 93 (1970).
[16] J. J. Szymanski, P. D. Barnes, G. E. Diebold, R. A. Eisenstein, G. B. Franklin, R. Grace, D. W. Hertzog, C. J. Maher, B. P. Quinn, R. Rieder, J. Seydoux, W. R. Wharton, S. Bart, R. E. Chrien, P. Pile, R. Sutter, Y. Xu, R. Hackenburg, E. V. Hungerford, T. Kishimoto, L. G. Tang, B. Bassalleck, and R. L. Stearns, Phys. Rev. C **43**, 849 (1991).
[17] R. Grace, P. D. Barns, R. A. Eisenstein, G. B. Franklin, C. Maher, R. Reider, J. Seydoux, J. Szymanski, W. Wharton, S. Bart, R. E. Chrien, P. Pile, Y. Xu, R. Hackenburg, E. Hungerford, B. Bassalleck, M. Barlett, E. C. Milner, and R. L. Stearns, Phys. Rev. Lett. **55**, 1055 (1985).
[18] K. J. Nield, T. Bowen, G. D. Cable, D. A. DeLise, E. W. Jenkins, R. M. Kalbach, R. C. Noggle, and A. E. Pifer, Phys. Rev. C **13**, 1263 (1976).
[19] J. P. Bocquet, M. Epherre-Rey-Campagnolle, G. Ericsson, T. Johansson, J. Konijn, T. Krogulski, M. Maurel, E. Monnand, J. Mougey, H. Nifenecker, P. Perrin, S. Polikanov, C. Ristori, and G. Tibell, Phys. Lett. B **192**, 312 (1987); **182**, 146 (1986).
[20] T. A. Armstrong, J. P. Bocquet, G. Ericsson, T. Johansson, T. Krogulski, R. A. Lewis, F. Malek, M. Maurel, E. Monnand, J. Mougey, H. Nifenecker, J. Passaneau, P. Perrin, S. M. Polikanov, M. Rey-Campagnolle, C. Ristori, G. A. Smith, and G. Tibell, Phys. Rev. C **47**, 1957 (1993).
[21] V. I. Noga, Yu. N. Ranyuk, N. Ya. Rutkevich, P. V. Sorokin, and E. V. Sheptulenko, Yad. Fiz. **43**, 1332 (1986) [Sov. J. Nucl. Phys. **43**, 856 (1986)].
[22] H. Ohm, T. Hermes, W. Borgs, H. R. Koch, R. Maier, D. Piasuhn, H. J. Stein, O. W. B. Schutt, K. Pysz, Z. Rudy, L. Jarczyk, B. Kamys, P. Kulessa, A. Strzalkowski, W. Cassing, Y. Vozumi, and I. Zychor, Phys. Rev. C **55**, 3062 (1997).
[23] P. Kulessa, K. Pysz, I. Zychor, Z. Rudy, H. Ohm, B. Kamys, M. Hartmann, W. Cassing, H. R. Koch, A. Strzalkowski, H. Hodde, W. Borgs, R. Maier, D. Prasuhn, M. Motoba, and O. W. B. Schult, Nucl. Phys. **A639**, 283c (1998).
[24] H. C. Bhang, S. Ajimura, K. Aoki, T. Hasegawa, O. Hashimoto, H. Hotchi, Y. D. Kim, T. Kishimoto, K. Maeda, H. Noumi, Y. Ohta, K. Omata, H. Outa, H. Park, Y. Sato, M. Sekimoto, T. Shibata, T. Takahashi, and M. Youn, Phys. Rev. Lett. **81**, 4321 (1998); Nucl. Phys. **A639**, 269c (1998).
[25] K. H. Tanaka, Nucl. Phys. **A450**, 533c (1986).
[26] T. Fukuda, T. Hasegawa, O. Hashimoto, A. Higashi, S. Homma, T. Kitami, Y. Matsuyama, T. Miyachi, T. Morimoto, T. Nagae, K. Omata, M. Sekimoto, T. Shibata, H. Sakaguchi,

T. Takahashi, K. Aoki, Y. Doi, Y. Kondo, Y. Makida, M. Nomachi, H. Noumi, O. Sasaki, T. Shintomi, H. Bhang, H. Park, M. Youn, H. Yu, Y. Gavrilov, S. Ajimura, T. Kishimoto, A. Ohkusu, N. Shinkai, K. Maeda, and R. Sawafta, Nucl. Instrum. Methods Phys. Res. A **361**, 485 (1995).

[27] T. Hasegawa, O. Hashimoto, S. Homma, T. Miyachi, T. Nagae, M. Sekimoto, T. Shibata, H. Sakaguchi, T. Takahashi, K. Aoki, H. Noumi, H. Bhang, M. Youn, Y. Gavrilov, S. Ajimura, T. Kishimoto, A. Ohkusu, K. Maeda, R. Sawafta, and R. P. Redwine, Phys. Rev. C **53**, 1210 (1996).

[28] T. Hasegawa, O. Hashimoto, S. Homma, T. Miyachi, T. Nagae, M. Sekimoto, T. Shibata, H. Sakaguchi, T. Takahashi, K. Aoki, H. Noumi, H. Bhang, M. Youn, Y. Gavrilov, S. Ajimura, T. Kishimoto, A. Ohkusu, K. Maeda, R. Sawafta, and R. P. Redwine, Phys. Rev. Lett. **74**, 224 (1995).

[29] GEANT: Detector Description and Simulation Tool, CERN Program Library, 1995.

[30] Y. D. Kim, H. Bhang, O. Hashimoto, K. Maeda, K. Omata, H. Outa, H. Park, and M. Youn, Nucl. Instrum. Methods Phys. Res. A **372**, 431 (1996).

[31] W. Braunschweig, E. Koenigs, W. Sturm, and W. Wallraff, Nucl. Instrum. Methods **134**, 261 (1976); G. D'Agostini, G. Marini, G. Martellotti, E. Massa, A. Rambaldi, and A. Sciubba, Nucl. Instrum. Methods Phys. Res. **185**, 49 (1981); T. Tanimori, T. Kageyama, K. Nakamura, M. Yoshioka, J. Haba, H. Kawai, M. Kobayashi, T. S. Nakamura, and N. Sasao, *ibid.* **216**, 57 (1983).

[32] R. H. Dalitz, D. H. Davis, and D. N. Tovee, Nucl. Phys. **A450**, 311c (1986); T. Cantwell, D. H. Davis, D. Kielczewska, J. Zakarzenski, M. Juric, U. Krecker, G. Coremans-Bertrant, J. Salton, T. Tymieniecka, A. Montwill, and P. Moriarty, *ibid.* **A236**, 445 (1974).

[33] P. H. Pile, S. Bart, R. E. Chrien, D. J. Millener, R. J. Sutter, N. Tsoupas, J.-C. Peng, C. S. Mishra, E. V. Hungerford, T. Kishimoto, L.-G. Tang, W. von Witsch, Z. Xu, K. Maeda, D. Gill, R. McCrady, B. Quinn, J. Seydoux, J. W. Sleight, R. L. Stearns, H. Plendl, A. Rafatian, and J. Reidy, Phys. Rev. Lett. **66**, 2585 (1991).

[34] T. Awaya, Nucl. Instrum. Methods **174**, 237 (1980).

[35] E. Oset and L. L. Salcedo, Nucl. Phys. **A443**, 704 (1985).

[36] A. Ramos, E. Oset, and L. L. Salcedo, Phys. Rev. C **50**, 2314 (1994).

[37] K. Itonaga, T. Ueda, and T. Motoba, Nucl. Phys. **A639**, 329c (1998).

[38] K. Itonaga (private communication).